Polarization dynamics in nonlinear anisotropic fibers

Andrey Komarov,[1] Konstantin Komarov,[1] Dmitry Meshcheriakov,[1] Foued Amrani,[2] and François Sanchez[2]
[1]*Institute of Automation and Electrometry, Russian Academy of Sciences, Acad. Koptyug Pr. 1, RU-630090 Novosibirsk, Russia*
[2]*Laboratoire de Photonique d'Angers EA 4644, Université d'Angers, 2 boulevard Lavoisier, F-49000 Angers, France*
(Received 11 March 2010; published 13 July 2010)

We give an extensive study of polarization dynamics in anisotropic fibers exhibiting a third-order index nonlinearity. The study is performed in the framework of the Stokes parameters with the help of the Poincaré sphere. Stationary states are determined, and their stability is investigated. The number of fixed points and their stability depend on the respective magnitude of the linear and nonlinear birefringence. A conservation relation analogous to the energy conservation in mechanics allows evidencing a close analogy between the movement of the polarization in the Poincaré sphere and the motion of a particle in a potential well. Two distinct potentials are found, leading to the existence of two families of solutions, according to the sign of the total energy of the equivalent mechanical system. The mechanical analogy allows us to fully characterize the solutions and also to determine analytically the associated beat lengths. General analytical solutions are given for the two families in terms of Jacobi's functions. The intensity-dependent transmission of a fiber placed between two crossed polarizers is calculated. Optimal conditions for efficient nonlinear switching compatible with mode-locking applications are determined. The general case of a nonlinear fiber ring with an intracavity polarizer placed between two polarization controllers is also considered.

DOI: 10.1103/PhysRevA.82.013813 PACS number(s): 42.81.−i, 42.55.Wd, 42.65.Sf

I. INTRODUCTION

Although the optical Kerr effect in single-mode fibers is commonly used for many applications involving passive mode locking based on nonlinear polarization evolution [1–13], modulational instability [14,15], or soliton propagation [16], there are few studies concerning the exact polarization dynamics when nonlinearity and birefringence are simultaneously present. As a matter of fact, in a recent article, Ding and Kutz had similar conclusions concerning the underlying theory of a passive polarizer used to mode lock a fiber laser [10].

Modulation instability in optical fibers has a long history. However, the peculiarities related to the vectorial nature of an electromagnetic wave have been rarely investigated. The majority of theoretical studies are based on the scalar nonlinear wave equation. The interplay between birefringence, nonlinearity, and dispersion was first studied in [17], where the polarization instability is predicted in the normal dispersion regime. In [18], the authors report the generation of ultrahigh-repetition-rate solitonlike pulse trains as a consequence of the interplay between the natural and nonlinear birefringence. In the case of passively mode locked fiber lasers, fully vectorial models [4–9] include both polarization effects and birefringence along the fiber, but no attempt is given to the exact evolution of the polarization state. Scalar models generally ignore the birefringence [12,13] or simply treat them as a perturbation [11]. Many authors merely explain that the optical Kerr effect induces an intensity-dependent rotation of the polarization ellipse, leading to intensity-dependent losses after a suitably oriented polarizer. This is true if the fiber is isotropic but can be completely false when the linear birefringence takes place. In practice, residual birefringence is always present, and the resulting beat length can be as low as 10 cm, as reported from magneto-optic measurements in Nd-doped fibers [19]. As a consequence, assuming a fiber length of about 20 m in standard fiber lasers, the length of the doped fiber spans from about the beat length (for weakly birefringent fibers) to several hundred times the beat length (for highly birefringent fibers). Therefore the interplay between the natural and the nonlinear birefringence as well as the resulting peculiarities on the mode-locking behavior deserve specific study. Before treating the full problem of a fiber laser with gain, dispersion, birefringence, and optical Kerr nonlinearity, it is of great importance to perform an extensive study of the properties of a wave which travels along a single-mode nonlinear birefringent fiber. This is the main objective of this article. As said previously, there are few results on this domain. An attempt to derive a formula for the nonlinear transmission of a nonlinear birefringent fiber placed between two crossed polarizers is reported in [20]. The authors consider the natural birefringence of the fiber but neglect the four-wave mixing terms of the optical Kerr nonlinearity. The range of validity is then seriously restricted because the nonlinear polarization coupling is due to the neglected term. In spite of that, the simplicity of the resulting nonlinear transmission formula makes it attractive for the description of some aspects of soliton fiber ring lasers [21,22]. A more realistic approach has been pioneered by Winful and colleagues, who really initiated this domain [23–25]. In these articles, the approach was based on the evolution of the two circular polarization components which are the polarization eigenstates of a purely Kerr medium. Winful pointed out the saddle-point instability for a polarization parallel to the fast axis of a birefringent fiber [23] and found one particular analytical solution to the nonlinear propagation problem. He also noted the analogy with a mechanical oscillator and investigated the nonlinear transmission of a birefringent nonlinear fiber placed between two orthogonal polarizers. This latter point is essential to the optimization of the nonlinear losses for efficient mode locking. Although the work of Winful is considerable and gives physical insight to many aspects of the propagation of a wave in a birefringent nonlinear medium, it is not fully satisfactory. For instance, the mechanical analogy is just mentioned [24], and only one analytical solution is given, while there are two

distinct families of solutions. Our ambition in this article is to provide an extensive study of the propagation of a wave in a birefringent nonlinear medium. For that purpose, we adopt a new approach to this task. The problem is formulated in the framework of the Stokes parameters and the Poincaré sphere.

This article is organized as follows. In Sec. II, we consider the evolution of a wave in a nonlinear anisotropic fiber and derive the evolution equations of the Stokes parameters. Section III is devoted to the topology of the solutions in the Poincaré sphere. It is demonstrated that the movement in the Poincaré sphere in the general case is a rotation around an instantaneous axis which depends on both the optical intensity and the surface of the polarization ellipse. Four fixed points are found in the Poincaré sphere. Two correspond to the eigenaxis of the anisotropic fiber, while the other two are intensity dependent and only exist if the nonlinear birefringence is greater than the natural birefringence. The stability of the stationary points is then analyzed. In agreement with [18], it is demonstrated that the point associated with the fast axis is an unstable saddle point. Local solutions are given for all fixed points. The mechanical analogy is investigated in Sec. IV. We first show that the evolution of the representative point in the Poincaré sphere is analogous to a movement of a particle in a potential well. Depending on the initial conditions, the potential may have one or two minima. We demonstrate that depending on the total energy of the particle, two physically different families of solutions occur. The first family exists only when the nonlinear birefringence is greater than the linear one and the sign of the ellipticity does not change; it is a rotating solution. The second family always exists and corresponds to an oscillating solution in which the sign of the ellipticity is periodically changed. Analytic solutions are found for both solutions in terms of Jacobi's functions. Their properties are examined in Sec. V. In particular, we show that the modulus of the Jacobian function is related to the initial conditions (i.e., initial polarization state). In Sec. VI, we consider the nonlinear losses associated with a birefringent nonlinear fiber placed between two crossed polarizers. The nonlinear transmission is derived with the help of the Mueller matrices. Optimization of the nonlinear transmission for efficient mode locking is performed. The general case is also considered. We demonstrate that maximum transmission discrimination between low and high intensity is obtained when the corresponding polarization states are located at opposite ends of any diameter in the Poincaré sphere.

II. THE STOKES PARAMETERS AND THE POINCARÉ SPHERE

We consider a monochromatic plane wave propagating in a fiber which is assumed to be lossless, anisotropic, and nonlinear (Kerr effect). At steady state and in the framework of the eigenaxis of the fiber, the electric field components are coupled through the following nonlinear equations:

$$\begin{aligned}\frac{du}{dz} &= iku + iq\left(|u|^2u + \frac{2}{3}|v|^2u + \frac{1}{3}v^2u^*\right),\\ \frac{dv}{dz} &= -ikv + iq\left(|v|^2v + \frac{2}{3}|u|^2v + \frac{1}{3}u^2v^*\right),\end{aligned} \tag{1}$$

where u and v are the slowly varying envelopes along the slow and fast axis ($k > 0$), respectively; k is the birefringent parameter; and q is the nonlinear parameter related to the nonlinear index coefficient (for focusing nonlinearity $q > 0$). Let us recall that the nonlinear term contains, by appearance order in Eqs. (1), the self-phase modulation term, the crossed-phase modulation term, and the four-wave mixing term.

The conservation of the energy during the propagation leads to the conservation relation

$$|u(z)|^2 + |v(z)|^2 = \text{const} = I. \tag{2}$$

In order to simplify Eq. (1), let us introduce the new variables

$$\begin{aligned}u &= U\sqrt{I}e^{iqIz},\\ v &= V\sqrt{I}e^{iqIz}.\end{aligned} \tag{3}$$

System (1) becomes

$$\begin{aligned}\frac{dU}{dz} &= ikU - i\Omega(|V|^2U - V^2U^*),\\ \frac{dV}{dz} &= -ikV - i\Omega(|U|^2V - U^2V^*),\end{aligned} \tag{4}$$

where $\Omega = qI/3$. With the new variables, the electric field is normalized to unity: $|U|^2 + |V|^2 = 1$.

For the analysis, it is convenient to introduce the Stokes parameters of the electric field. They are defined by [26]

$$\begin{aligned}S_0 &= |U|^2 + |V|^2 = 1,\\ S_1 &= |U|^2 - |V|^2,\\ S_2 &= UV^* + U^*V = 2|U||V|\cos\varphi,\\ S_3 &= -i(UV^* - U^*V) = 2|U||V|\sin\varphi,\end{aligned} \tag{5}$$

where $\varphi = \varphi_u - \varphi_v$ is the phase difference between the two electric field components.

The Stokes parameters are not independent; they verify the conservation relation

$$S_0^2 = S_1^2 + S_2^2 + S_3^2. \tag{6}$$

The Stokes parameters completely determine the state of the polarization of the wave. They can be written using the azimuth ψ of the polarization and the angle of ellipticity χ:

$$\begin{aligned}S_1 &= \cos 2\psi\cos 2\chi,\\ S_2 &= \sin 2\psi\cos 2\chi,\\ S_3 &= \sin 2\chi.\end{aligned} \tag{7}$$

All possible polarization states are obtained for $\psi \in [0,\pi]$ and $\chi \in [-\pi/4,\pi/4]$. When ψ and χ vary, the point representative of the vector $\vec{S} = (S_1,S_2,S_3)^t$ describes a unit sphere which is the well-known Poincaré sphere (the superscript t stands for the transpose vector, i.e., the column vector). With our definition of the Stokes parameters, the Northern (Southern) hemisphere is associated with right-handed (left-handed) polarizations. The Poincaré sphere is illustrated in Fig. 1. Hence the evolution of the state of the polarization along the fiber can be represented by the movement of a point on a unit

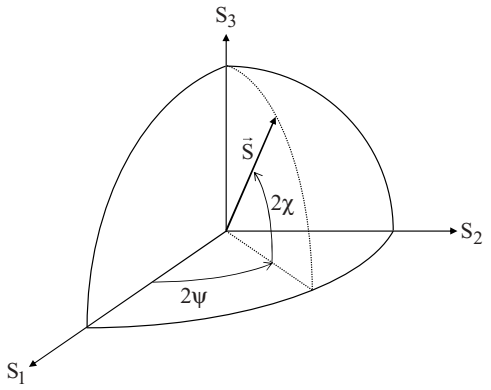

FIG. 1. The Poincaré sphere.

sphere. Using the Stokes parameters Eqs. (4) are written in the form

$$\begin{aligned} \frac{dS_1}{dz} &= 2\Omega S_2 S_3, \\ \frac{dS_2}{dz} &= -2kS_3 - 2\Omega S_1 S_3, \\ \frac{dS_3}{dz} &= 2kS_2. \end{aligned} \tag{8}$$

III. TOPOLOGY OF THE SOLUTIONS

A. Case with no natural birefringence

We first consider the case where there is no natural birefringence, that is, $k = 0$. Under such circumstances, Eqs. (8) become

$$\begin{aligned} \frac{dS_1}{dz} &= 2\Omega S_2 S_3, \\ \frac{dS_2}{dz} &= -2\Omega S_1 S_3, \\ \frac{dS_3}{dz} &= 0. \end{aligned} \tag{9}$$

The last equation shows that $S_3 = \text{const}$, which means that the surface of the polarization ellipse remains constant during the propagation [12]. Equation (9) can be written in vector form as

$$\frac{d\vec{S}}{dz} = -2S_3\vec{\Omega} \wedge \vec{S}, \tag{10}$$

where $\vec{\Omega} = (0\ 0\ \Omega)^t$ and $\vec{S} = (S_1\ S_2\ S_3)^t$.

Relation (10) demonstrates that the movement of $\vec{S}$ is a rotation around the S_3 axis at the angular frequency $2S_3\Omega$ (this results from a simple and direct analogy with a particle with a circular motion around a fixed axis). Then $\vec{S}$ has a circular motion around the S_3 axis on the Poincaré sphere. If $S_3 > 0$, the movement is clockwise, while if $S_3 < 0$, it is anticlockwise. This is illustrated in Fig. 2. The equatorial plane is the boundary between these opposite circular rotations. In the equatorial plane, $S_3 = 0$ and the polarization state is linear. As a consequence, the polarization is not modified along the propagation because the angular frequency of rotation vanishes.

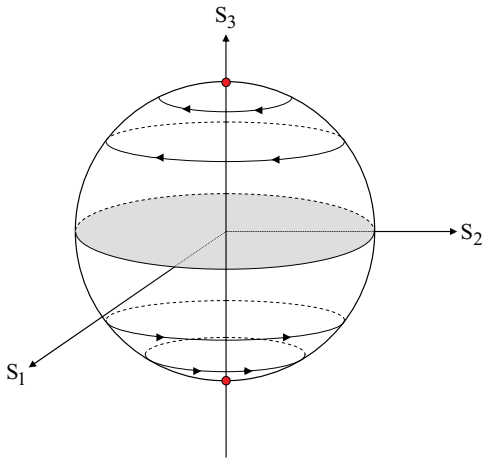

FIG. 2. (Color online) Evolution of the polarization state with no natural birefringence. The points in the poles are stationary states.

Relation (10) allows us also to determine the stationary points (or fixed points) which correspond to the polarization eigenstates of the nonlinear fiber. In addition to any linear polarization which does not undergo a variation during propagation, the states for which $S_1 = S_2 = 0$ are also stationary because in this case $d\vec{S}/dz$. Because of the normalization of the vector $\vec{S}$, the corresponding projection on the S_3 axis is $S_3 = \pm 1$. Therefore the fixed points are the poles and physically correspond to the right (North Pole) and left (South Pole) circular polarizations. The fiber behaves like a circular birefringent medium. If the incident polarization is circular, it propagates without any change. If the incident polarization is right (left) handed, the trajectory of the polarization state in the Poincaré sphere is clockwise (anticlockwise) around the North (South) Pole. The trajectories in the Poincaré sphere do not depend on the intensity or on the polarization eigenstates. However, the frequency of rotation depends linearly on the optical intensity (through Ω) and on the surface of the polarization ellipse S_3, which is a conserved quantity during the propagation.

B. General case

1. Stationary states

In the general case, we have to consider Eqs. (8) without any simplification. It is easy to show that Eqs. (8) can be written in vector form as

$$\frac{d\vec{S}}{dz} = 2\vec{k} \wedge \vec{S} - 2S_3\vec{\Omega} \wedge \vec{S}, \tag{11}$$

where $\vec{k} = (k,0,0)^t$ and $\vec{\Omega} = (0,0,\Omega)^t$. Relation (11) shows that the evolution of $\vec{S}$ is a rotation around the axis $\vec{k} - S_3\vec{\Omega}$. However, the exact evolution is not a simple rotation because the axis of rotation depends on the coordinate S_3. Therefore $\vec{k} - S_3\vec{\Omega}$ defines the instantaneous axis of rotation. Relation (11) also shows that the nonlinear fiber is a medium exhibiting a natural linear birefringence (*linear* is used here in the sense that the polarization eigenstates are two orthogonal linear polarizations) and a circular birefringence resulting from optical Kerr nonlinearity.

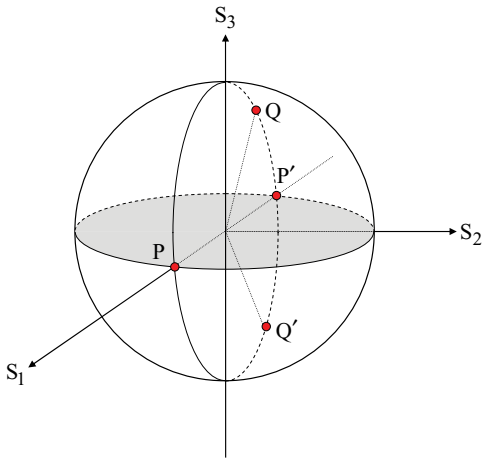

FIG. 3. (Color online) Stationary solutions in the general case.

The trajectories can be better identified if we first look for the stationary solution, that is, fixed points in the Poincaré sphere. From Eqs. (8), we get

$$\begin{aligned} S_2 &= 0, \\ (\Omega S_1 + k) S_3 &= 0. \end{aligned} \tag{12}$$

The first relation demonstrates that the fixed points are in the plane (S_1, S_3). The second relation leads to two different solutions:

$$S_3 = 0, \tag{13a}$$

$$S_1 = -\frac{k}{\Omega}. \tag{13b}$$

Taking into account that $\|\vec{S}\| = 1$, we find four fixed points in the Poincaré sphere. Their coordinates are as follows:

$$P \begin{vmatrix} 1 \\ 0 \\ 0 \end{vmatrix} \quad P' \begin{vmatrix} -1 \\ 0 \\ 0 \end{vmatrix} \quad Q \begin{vmatrix} -k/\Omega \\ 0 \\ \sqrt{1-k^2/\Omega^2} \end{vmatrix} \quad Q' \begin{vmatrix} -k/\Omega \\ 0 \\ -\sqrt{1-k^2/\Omega^2} \end{vmatrix}. \tag{14}$$

Figure 3 shows the localization of the stationary points in the Poincaré sphere.

From Eq. (14), one can deduce that the polarization eigenstates P and P' exist for any value of the parameters. This is not the case for the solutions Q and Q', which exist only if $k \leqslant \Omega$. Solutions P and P' physically correspond to the polarization eigenstates of the fiber with linear birefringence: P is the eigenmode associated with the linear polarization parallel to the slow axis, while P' corresponds to the fast axis polarization eigenmode. An incident polarization parallel to one of the eigenaxis of the fiber remains in the same state because the linear anisotropy does not modify it, and as a consequence, it does not undergo nonlinear effects because the surface of the polarization ellipse remains equal to zero. The solutions Q and Q' correspond to the polarization eigenstates of the fiber in the presence of the optical Kerr effect. These eigenstates are elliptic polarizations with the same azimuth but opposite ellipticity (note that they are not orthogonal polarizations since their representations in the Poincaré sphere are not two diametrically opposite points). The fact that these solutions exist only for $k \leqslant \Omega$ demonstrates that if the linear anisotropy is greater than the nonlinear anisotropy, then the natural polarization eigenmodes are not modified, and one can expect that the efficiency of mode locking will be considerably changed. If we recall that the nonlinear anisotropy Ω depends on the intensity I, and previous situation occurs below some value of the intensity, there is a threshold for the emergence of new intensity-dependent polarization eigenstates. The latter take place for $I > 3k/q$.

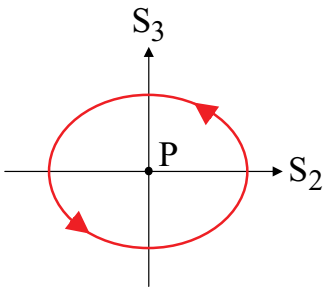

FIG. 4. (Color online) Trajectory around the stationary point P.

2. *Movement in the vicinity of P*

To investigate the evolution of $\vec{S}$ around the stationary point P, we assume that $S_1 \approx 1$ and $|S_2|, |S_3| \ll 1$. Equations (8) reduce to

$$\begin{aligned} \frac{dS_2}{dz} &= -2(k+\Omega) S_3, \\ \frac{dS_3}{dz} &= 2k S_2. \end{aligned} \tag{15}$$

System (15) has a periodic solution with a rotation frequency $\Omega_P = 2\sqrt{k(k+\Omega)}$. Therefore the point representative of the polarization state has a left-handed periodic movement around P, as illustrated in Fig. 4. The trajectories of the movement are given by $S_2^2/(k+\Omega) + S_3^2/k = \text{const}$, which are ellipses. The ratio of the semimajor axis of the ellipse (S_2 direction) to the semiminor one (S_3 direction) is equal to $\sqrt{1+\Omega/k}$.

3. *Movement in the vicinity of P′*

In this case, we assume that $S_1 \approx -1$ and $|S_2|, |S_3| \ll 1$. Equations (8) reduce to

$$\begin{aligned} \frac{dS_2}{dz} &= -2(k-\Omega) S_3, \\ \frac{dS_3}{dz} &= 2k S_2. \end{aligned} \tag{16}$$

The eigenvalues of the associated matrix are $\lambda = \pm 2i\sqrt{k(k-\Omega)}$. We have thus to consider two different cases. If $k > \Omega$, the eigenvalues are imaginary and there is a periodic movement around P' at the frequency $\Omega_{P'} = 2\sqrt{k(k-\Omega)}$. The trajectories are ellipses. The ratio of the semiminor axis of the ellipse (S_2 direction) to the semimajor one (S_3 direction) is equal to $\sqrt{1-\Omega/k}$. Otherwise, if $k \leqslant \Omega$, the eigenvalues are real, and the point P' can be attractive, repulsive, or both. The nature of the stationary point is determined with the sign of the derivatives. If $(S_2 > 0, S_3 > 0)$ or $(S_2 < 0, S_3 < 0)$, P' is repulsive, while if $(S_2 < 0, S_3 > 0)$ or $(S_2 > 0, S_3 < 0)$, P' is attractive. P' is therefore a saddle point, as evidenced in [24].

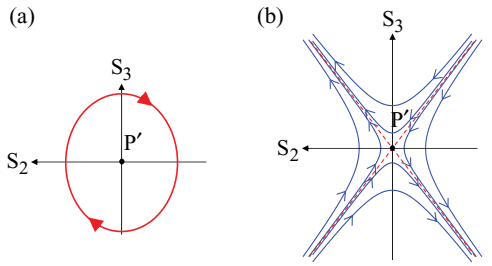

FIG. 5. (Color online) Trajectories around the stationary point P'. (a) Elliptic motion when $k > \Omega$. (b) Hyperbolic motion when $k \leqslant \Omega$. The dashed lines are the asymptotes.

Trajectories can be easily calculated from Eq. (16). They can be put in the form

$$\frac{S_2^2}{\Omega - k} - \frac{S_3^2}{k} = \text{const.} \tag{17}$$

Trajectories are therefore hyperbolas with oblique asymptotes. The equations of the asymptotes are $S_3 = \pm\sqrt{k/(\Omega - k)}S_2$, and they cross at the saddle point. The trajectories in both cases, $k > \Omega$ and $k \leqslant \Omega$, are illustrated in Fig. 5.

4. Movement in the vicinity of Q

Solution Q is restricted to the case $k \leqslant \Omega$. We consider small variations around the solution Q: $\delta\vec{S} = \vec{S} - \vec{S}_Q$, where $\vec{S}_Q$ is the vector associated with the stationary solution Q. Assuming that $\|\delta\vec{S}\| \ll 1$, Eqs. (8) can be rewritten in the form

$$\begin{aligned} \frac{d\delta S_1}{dz} &= 2\Omega S_{3Q}\delta S_2, \\ \frac{d\delta S_2}{dz} &= -2\Omega S_{3Q}\delta S_1, \\ \frac{d\delta S_3}{dz} &= 2k\delta S_2, \end{aligned} \tag{18}$$

where $S_{3Q} = \sqrt{1 - k^2/\Omega^2}$. The eigenvalues of the associated matrix are $\lambda_{1,2} = \pm 2i\Omega S_{3Q}, \lambda_3 = 0$. This means that there is a periodic movement around Q at the frequency $\Omega_Q = 2\sqrt{\Omega^2 - k^2}$. From the first and second Eqs. (18), one can see that the projection of the closed movement trajectory into the plane (S_1, S_2) is a circle. That means that the corresponding trajectory on the Poincaré sphere is an ellipse. The minor axis of the ellipse is along the S_2 axis, and the major one lies in the plane (S_1, S_3). The ratio of the former to the latter is equal to $\sqrt{1 - k^2/\Omega^2}$. The point representative of the polarization state has a right-handed periodic movement around Q.

5. Movement in the vicinity of Q′

The analysis is analogous to that performed in the case of the fixed point Q. Results are analogous in both cases Q' and Q. The point representative of the polarization state has a right-handed elliptical movement around Q'. The rotation frequency is $\Omega_{Q'} = 2\sqrt{\Omega^2 - k^2}$. The ratio between the lengths of the principal axis of the ellipse is equal to $\sqrt{1 - k^2/\Omega^2}$. These results are obvious if we keep in mind the invariance of Eqs. (8) under the transformation $S_3 \to -S_3, z \to -z$. As a consequence of this invariance, the trajectories on the Poincaré sphere are symmetrical with respect to the plane $S_3 = 0$. There exists also the equivalent symmetry for trajectories pictured with respect to the plane $S_2 = 0$.

IV. MECHANICAL ANALOGY

A. Basic equations

Following the suggestion of Winful [24], we fully develop the mechanical analogy existing between the polarization evolution in the Poincaré sphere and a particle moving in a potential well. Substituting S_2 from the third Eq. (8) into the first one, we obtain the conservation of the quantity:

$$J = kS_1 - \Omega\frac{S_3^2}{2} = \text{const.} \tag{19}$$

From the second and third Eqs. (8), one can write the following equation:

$$\frac{d^2S_3}{dz^2} = -4k(k + \Omega S_1)S_3. \tag{20}$$

Using Eq. (19), we can rewrite Eq. (20) in the form

$$\frac{d^2S_3}{dz^2} = \left[-4(J\Omega + k^2) - 2\Omega^2 S_3^2\right] S_3 = -\frac{dU(S_3)}{dS_3}. \tag{21}$$

This equation coincides with the equation describing the movement of a particle of unit mass in a potential well $U = U(S_3)$ (S_3 plays the role of the coordinate variable and z of the temporal variable), where

$$U(S_3) = 2(J\Omega + k^2)S_3^2 + \frac{\Omega^2}{2}S_3^4. \tag{22}$$

The form of the potential well $U(S_3)$ depends on both the initial coordinate and the velocity of the particle (on initial area of the polarization ellipse and its orientation) because these parameters determine the conserved value J in Eq. (22). Equation (21) describes the evolution of the S_3 component of a point moving on the unit sphere shown in Fig. 1. For the particle moving in the potential well $U(S_3)$, it leads to the conservation of the total energy W, including kinetic and potential parts:

$$\begin{aligned} W &= \frac{1}{2}\left(\frac{dS_3}{dz}\right)^2 + U(S_3) \\ &= \frac{1}{2}\left(\frac{dS_3}{dz}\right)^2 + 2(J\Omega + k^2)S_3^2 + \frac{\Omega^2}{2}S_3^4 = \text{const.} \end{aligned} \tag{23}$$

The value of the total energy W determines the trajectory (trajectories around the fixed points Q, Q' or P, P').

Thus the evolution of the polarization ellipse during the propagation of radiation in a nonlinear anisotropic fiber is similar to the evolution dynamics of a particle moving in a potential well. This analogy enables a simple way to describe conditions for a realization of various regimes of a polarization evolution through an initial state of radiation. An equation for S_1, analogous to Eq. (21), can also be obtained:

$$\frac{d^2S_1}{dz^2} = 4k(\Omega + 4J) - 8(2k^2 - \Omega J)S_1 - 12\Omega k S_1^2. \tag{24}$$

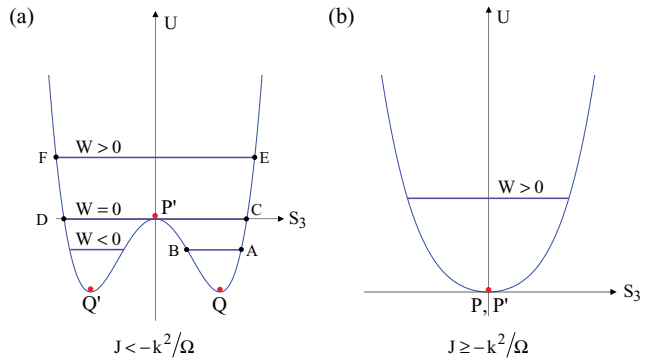

FIG. 6. (Color online) Potential associated with the evolution of the S_3 component of the polarization state during the propagation along the fiber. (a) The initial conditions are such that $J < -k^2/\Omega$. Depending on the total energy, the trajectory in the Poincaré sphere is periodic around stationary points Q, Q' or P, P'. A, B, C, D, E, F, and P' are turning points. (b) The initial conditions are such that $J \geqslant -k^2/\Omega$. The total energy is positive, and the trajectories in the Poincaré sphere are periodic around point P, P'.

B. Analysis of the evolution of the polarization on the basis of mechanical analogy

1. *General properties of the evolution*

Depending on the initial conditions, and then on the value of J, there are two distinct potential forms $U(S_3)$. Indeed, if $J < -k^2/\Omega$ (case a), the potential has two minima and one maximum, while if $J \geqslant -k^2/\Omega$ (case b), the potential $U(S_3)$ exhibits only one minimum. The two situations are depicted in Fig. 6. It can be easily checked that if $k < \Omega$, both potential curves can be obtained depending on initial conditions, while if $k \geqslant \Omega$, only the potential with one minimum occurs. The minima (maxima) correspond to the stable (unstable) stationary points in the Poincaré sphere.

Let us first consider case a, where $J < -k^2/\Omega$. There exist several families of solutions depending on the total energy W. If $W < 0$, the trajectories are periodic around the points Q or Q' [(Q, Q') family of solutions]. For these trajectories, the sign of S_3 is conserved. That means that the sign of the ellipticity is conserved, that is, the sense of rotation of the electric field remains the same during the propagation along the fiber (the polarization ellipse rotates in a monotonic way, while the ellipticity varies). If $W > 0$, the trajectories are periodic above a potential barrier [(P, P') family of solutions]. The sign of S_3 is periodically changed. As a consequence, and in contrast with the case $W < 0$, the polarization ellipse oscillates around the slow or the fast axis, depending on the initial conditions. The maximum located at $S_3 = 0$ corresponds to the stationary saddle point P'. The case $W = 0$ corresponds to the boundary (or separatrix) between the (Q, Q') family and the (P, P') family. These two families are delimited by the asymptotes in the Poincaré sphere [see Fig. 5(b)].

Case b, where $J \geqslant -k^2/\Omega$, occurs always if $k \geqslant \Omega$. In this case, the energy is always positive, and the trajectories are periodic around points P or P' [(P, P') family]. Let us now determine the conditions for the realization of various types of polarization evolution. First of all, it is necessary to note that in turning points A, B, C, P', D, E, and F in Fig. 6, the velocity $dS_3/dz = 0$, and from the last relation of Eqs. (8), we obtain $S_2 = 0$, that is, $\varphi = \pm\pi/2$ in Eq. (5). This means that in these points, the principal axis of the polarization ellipse coincides with the eigenaxis of the fiber [Eq. (7) implies that the azimuth is $\psi = 0$ or $\psi = \pi/2$]. Thus any periodic evolution of the polarization ellipse can be obtained if an initial ellipse is taken with such orientation. The corresponding initial point z is then a turning point. In a turning point, the polarization ellipse is then fully characterized by the value S_1, which determines the ellipticity, and by the sign of S_3, which determines if the polarization is left handed or right handed. Each trajectory has two turning points, as shown in Fig. 6. The relation between parameters of the ellipses S_1 in two turning points Γ_1 and Γ_2 can be found from Eq. (19):

$$J = kS_{1\Gamma_2} - \Omega\frac{S_{3\Gamma_2}^2}{2} = kS_{1\Gamma_1} - \Omega\frac{S_{3\Gamma_1}^2}{2}. \tag{25}$$

Depending on the family of solutions, the turning points Γ_1 and Γ_2 will be A and B or E and F. Taking into account the relation $S_{1\Gamma_1,\Gamma_2}^2 + S_{3\Gamma_1,\Gamma_2}^2 = 1$, the quadratic algebraic equation (25) admits two solutions:

$$S_{1\Gamma_2} = \begin{cases} S_{1\Gamma_1}, \\ -2\dfrac{k}{\Omega} - S_{1\Gamma_1}. \end{cases} \tag{26}$$

Equations (26) determine the characteristics of the polarization ellipse in the second turning point through its properties in the first turning point.

2. *Polarization evolution for the (Q, Q') family of solutions*

The rotating solution is illustrated in Fig. 7, which shows the evolution of the polarization state along the fiber. The spatial period L_B is the beat length. In the case where $-2k/\Omega - S_{1A} > -1$, the ellipse with parameter S_{1A} in the first turning point transforms into the ellipse with parameter $S_{1B} = -2k/\Omega - S_{1A}$ in the second turning point. In turning point B (Fig. 6), S_3 is minimum, and $S_3 = S_{3\,\min}$ and corresponds to the greater magnitude from $S_{1\Gamma_1}$ or $S_{1\Gamma_2}$ [see Eq. (26)]. The state with $S_3 = S_{3\,\max}$ (point A in Fig. 6) corresponds the smaller one. Thus the condition for the realization of the rotating solution (S_3 never vanishes; $S_3 \neq 0$) can be rewritten in the form

$$2\frac{k}{\Omega} + S_{1A} < 1. \tag{27}$$

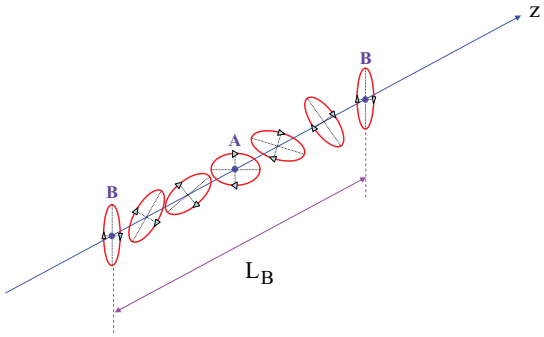

FIG. 7. (Color online) Evolution of the polarization state for the rotating solution. A and B are the turning points and L_B is the beat length.

The solution with $S = S_{3\min} = S_{3\max}$ (the bottoms of the potential well in Fig. 6 and the pole points Q, Q' in the unit sphere) is realized with $S_{1A} = -k/\Omega$. In this case, the polarization ellipse is stationary and does not rotate [see Eqs. (8) with $S_2 = 0$].

In the case of a weak linear anisotropy $k \ll \Omega$, we obtain from Eq. (26) $S_{1B} \approx -S_{1A}$. This means that the polarization ellipses are placed orthogonally relative to each other in the turning points (i.e., x and y have changed their roles: the semiminor axis of one coincides with the semimajor axis of the other). Equation (25) gives $S_{3\max} \approx S_{3\min}$. The frequency of the ellipse rotation resulting from Eqs. (8) with $k = 0$ coincides with the frequency of the change of the area S_3 in the vicinity of the bottom of the well, which is obtained from Eq. (21): $\Omega_{\rm osc} = 2\Omega S_{3\max}$.

At the boundary $S_{1A} = 1 - 2k/\Omega$, we get $S_{1B} = -1$, $S_{3\min} = 0$. This solution corresponds to the boundary (DC) which separates rotating solutions [(Q, Q') family] from oscillating solutions [(P, P') family].

From Eq. (23), and after some cumbersome algebra, we obtain the expression for a total spatial period of one oscillation, which corresponds to the beat length

$$L_B = \frac{2}{\Omega}\int_{S_{3\min}}^{S_{3\max}} \frac{dS_3}{\sqrt{(S_{3\max}^2 - S_3^2)(S_3^2 - S_{3\min}^2)}} = \frac{2}{\Omega S_{3\max}}\mathrm{K}(\kappa), \tag{28}$$

where $\mathrm{K}(\kappa) = \int_0^{\pi/2}(d\varphi/\sqrt{1-\kappa^2\sin^2\varphi})$ is the complete elliptic integral of a first kind and $\kappa^2 = (S_{3\max}^2 - S_{3\min}^2)/S_{3\max}^2$. The period of oscillation in the vicinity of the polar points Q, Q' is $L_{B_0} = \pi/\sqrt{\Omega^2 - k^2} = 2\pi/\Omega_{Q,Q'}$. Indeed, near Q or $Q', S_{3\max} \approx S_{3\min} \approx \sqrt{1-(\kappa/\Omega)^2}, \kappa \approx 0$, and $\mathrm{K}(0) = \pi/2$. For a solution in the vicinity of the boundary between the two families of solutions, $S_{3\min} \to 0, \kappa \to 1, \mathrm{K} \to \infty$, and the beat length diverges: $L_B \to \infty$. Assuming $S_{3\max} \approx S_{3Q} = \sqrt{1-(\kappa/\Omega)^2}$ in the denominator of Eq. (26), we obtain an approximate expression for the beat length, $L_B \approx 2\mathrm{K}(\kappa)/\sqrt{\Omega^2 - k^2}$, which is a useful expression to study the influence of κ. Results are given in Fig. 8, which points out that the beat length increases while the trajectory approaches the separatrix.

3. *Polarization evolution for the (P, P') family of solutions*

With breakdown of Eq. (27), oscillating solutions are realized. These solutions are the (P, P') solutions and are illustrated in Fig. 9, which shows the evolution of the polarization state along the fiber. An example of evolution in the (S_2, S_3) plane is given in Fig. 10(a), together with the notation used for the relevant points. (P, P') solutions are realized when $W > 0$ and the turning points are E and F [see Figs. 6 and 10(a)]. In this case, Eq. (26) gives $S_{1F} = S_{1E}$, but $S_{3F} = -S_{3E}$. All solutions of such kind can be obtained from a starting initial point G in the Poincaré sphere such that $S_{3G} = 0$ and with a variable parameter S_{1G}. That means that the initial polarization is taken in the equatorial plane (see Fig. 3) and is then a linear polarization. The azimuth of the initial polarization is equal to ψ_G ($S_{1G} = \cos 2\psi_G$).

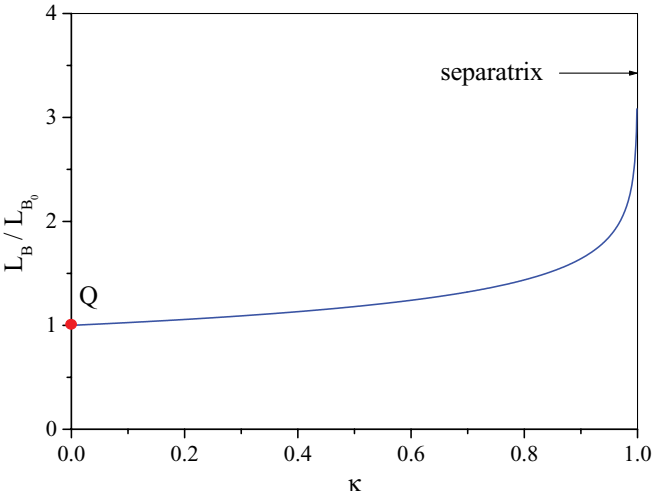

FIG. 8. (Color online) Approximate evolution of the beat length for the (Q, Q') family of solutions as a function of κ.

Let us now determine the state of polarization in relevant points of the trajectory. After a quarter period of the total oscillation the polarization area, S_3 becomes maximal $S_{3\max}$ [the turning point is E, as illustrated in Fig. 10(a), and the principal axes of the polarization ellipse are aligned with the eigenaxes of the fiber (x and y)]. From Eq. (19), we obtain

$$J = kS_{1G} = kS_{1E} - \Omega\frac{S_{3E,\max}^2}{2}. \tag{29}$$

With the help of the relation $S_{1E}^2 + S_{3E,\max}^2 = 1$, Eq. (29) yields the angle of the ellipticity χ_E:

$$S_{1E} = \cos 2\chi_E = -\frac{k}{\Omega} + \sqrt{\left(\frac{k}{\Omega}\right)^2 + 2\left(\frac{k}{\Omega}\right)\cos 2\Psi_G + 1}. \tag{30}$$

After a half period [point H in Fig. 10(a)], the field has again a linear polarization $S_{3H} = 0$. The polarization direction is determined by the azimuth $\psi_H = -\psi_G$ if $\psi_G < \pi/4$ and by the angle $\psi_H = \pi - \psi_G$ if $\psi_G > \pi/4$. After a three-quarter period, the area reaches the minimal size $S_{3\min} = -S_{3\max}$, which corresponds to the second turning point F. In this point, the polarization ellipse is the same as that of point E, except that the sense of rotation has changed because the ellipticity angle becomes the opposite of that of point E. After a total period, the polarization comes back to the initial linear state with the

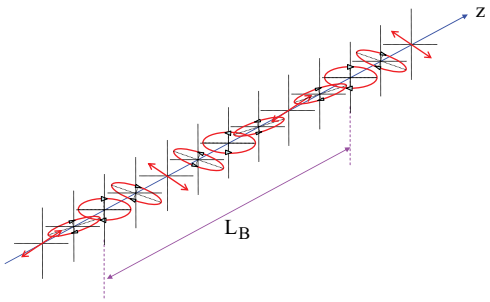

FIG. 9. (Color online) Evolution of the polarization state for the oscillating solution.

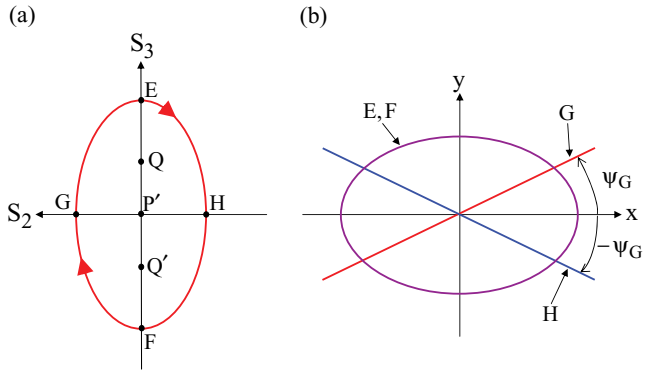

FIG. 10. (Color online) (a) Example of evolution around the point P' with points of interest. (b) Electric field polarization in the x-y plane corresponding to the relevant points G (linear polarization), E (right-handed elliptic polarization), H (linear polarization), and F (left-handed elliptic polarization).

angle $\psi = \psi_G$. Thus the semimajor axis of the polarization ellipse oscillates around the x axis between the ψ_G and $-\psi_G$ directions if $\psi_G < \pi/4$ [see Fig. 10(b)] or around the y axis between the ψ_G and $\pi - \psi_G$ directions if $\psi_G > \pi/4$. In the turning points, the polarization ellipse is aligned along the eigenaxis of the fiber.

The conservation of the energy in the mechanical analogy takes the form

$$2(J\Omega + k^2)S_3^2 + \frac{\Omega^2}{2}S_3^4 + \frac{1}{2}\left(\frac{dS_3}{dz}\right)^2 = \frac{1}{2}\left(\frac{dS_3}{dz}\Big|_G\right)^2, \tag{31}$$

with $J = kS_{1G} = k\cos 2\psi_G$ and $dS_3/dz|_G = 2kS_{2G} = 2k\sin 2\psi_G$. From Eq. (31), we obtain the expression for the spatial period of an oscillation (beat length):

$$L_B = \frac{4}{\Omega\sqrt{S_{3\max}^2 + |S_{3n}^2|}}\mathrm{K}(\kappa), \tag{32}$$

where $\kappa^2 = S_{3\max}^2/(S_{3\max}^2 + S_{3n}^2)$ and the values $S_{3\max}^2$ and S_{3n}^2 are the positive and negative roots of a square algebraic equation for S_3^2, respectively, which is obtained from Eq. (31):

$$\left(S_3^2\right)^2 + 4\left(\frac{k}{\Omega}\right)\left[\cos 2\psi_G + \left(\frac{k}{\Omega}\right)\right]S_3^2 - 4\left(\frac{k}{\Omega}\right)^2\sin 2\psi_G = 0, \tag{33}$$

$$S_{3\max,3n}^2 = -2\left(\frac{k}{\Omega}\right)\left[\cos 2\psi_G + \left(\frac{k}{\Omega}\right) \mp \sqrt{1 + 2\left(\frac{k}{\Omega}\right)\cos 2\psi_G + \left(\frac{k}{\Omega}\right)^2}\right]. \tag{34}$$

In the case of a movement in the vicinity of the polar point P, we obtain $S_{3\max} \to 0, S_{3n}^2 \to -4(k/\Omega)(1 + k/\Omega), \kappa \to 0$, and $L_B \approx \pi/\sqrt{k(k+\Omega)} = 2\pi/\Omega_P$. In the case of a movement in the vicinity of the saddle point $P'(k < \Omega)$, we obtain $S_{3\max}^2 \approx 4(k/\Omega)(1 - k/\Omega), S_{3n}^2 \to 0, \kappa \to 1, \mathrm{K} \to \infty$, and the beat length diverges as $L_B \to \infty$. Finally, for a movement

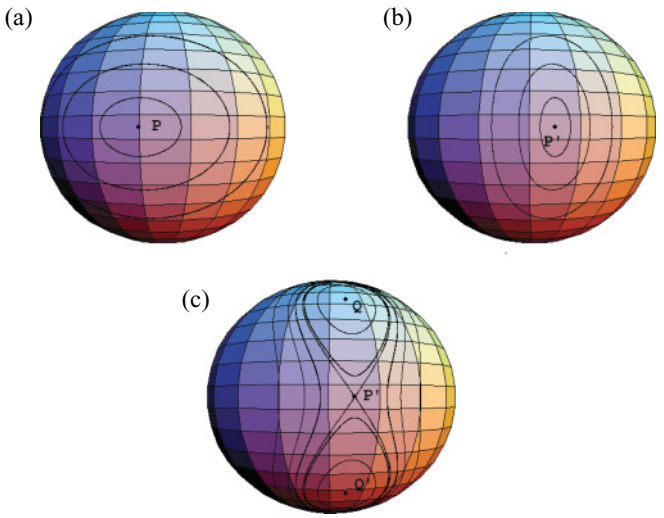

FIG. 11. (Color online) Evolution of the state of polarization in the Poincaré sphere. (a) Evolution around P when $k > \Omega$. (b) Evolution around P' when $k > \Omega$. (c) Case where $k < \Omega$. The double-loop curve is the boundary between Q-Q' solutions and P-P' solutions.

in the vicinity of the polar point $P'(k > \Omega)$, we obtain $S_{3\max}^2 \to 0, S_{3n}^2 \approx -4(k/\Omega)(k/\Omega - 1), \kappa \to 0, \mathrm{K} \to \pi/2$, and the period $L_B \approx \pi/\sqrt{k(k-\Omega)} = 2\pi/\Omega_{P'}$.

C. Numerical solutions in the Poincaré sphere

For sake of completeness, we give numerical solutions of Eqs. (8). The different evolutions are represented in the Poincaré sphere and are shown in Fig. 11. As was predicted in Sec. III, the movement is very close to elliptic motion in the case where $k > \Omega$. This is demonstrated in Figs. 11(a) and 11(b), which give the solutions around stationary points P and P'. In the case where $k < \Omega$, the results are shown in Fig. 11(c): If the initial conditions are such that the total energy is negative, the movement is periodic around points Q or Q', while if the initial conditions are taken in order to obtain a positive total energy W, the evolution is periodic around Q and Q'. The double-loop curve with a crossing at point P' corresponds to the separatrix between the two families of solutions. It is remarkable to note that similar trajectories in the Poincaré sphere were obtained in a very different problem, which concerned a nonlinear coupler [27]. In that case, the intensity-dependent fixed points were located in the equatorial plane because no photo-induced circular birefringence was taken into account.

V. EXACT SOLUTIONS

A. Properties of Jacobian functions

Equations (28) and (32), giving the period of oscillation, suggest that the evolution of the Stokes parameters (S_1, S_2, S_3) can be expressed through Jacobi's functions. Before proceeding, we briefly describe the basic properties of these functions [28]. The Jacobi's functions are determined through an incomplete elliptic integral of the first kind, $u(\varphi,\kappa) = \int_0^\varphi d\varphi/\sqrt{1-\kappa^2\sin^2\varphi}$, where φ and κ are the amplitude and the modulus of u, respectively ($\kappa^2 < 1$). The amplitude is generally written as $\varphi = \mathrm{am}\ u$. We now define the sine

amplitude sn $u = \sin\varphi$, the cosine amplitude cn $u = \cos\varphi$, and the delta amplitude dn $u = \sqrt{1-\kappa^2\sin^2\varphi} = d\varphi/du$. The functions sn u, cn u, and dn u are the Jacobi's functions. They verify the relations $\mathrm{sn}^2u + \mathrm{cn}^2u = 1, \mathrm{dn}^2u + \kappa^2\mathrm{sn}^2u = 1$, sn $0 = 0$, cn $0 = 1$, and dn $0 = 1$. The Jacobi's functions verify the following differential equations:

$$\begin{aligned}\frac{d}{du}\mathrm{sn}\,u &= \mathrm{cn}\,u\,\mathrm{dn}\,u,\\ \frac{d}{du}\mathrm{cn}\,u &= -\mathrm{sn}\,u\,\mathrm{dn}\,u,\\ \frac{d}{du}\mathrm{dn}\,u &= -\kappa^2\mathrm{sn}\,u\,\mathrm{cn}\,u.\end{aligned} \tag{35}$$

The oscillation period for sn u and cn u is $T = 4\mathrm{K}(\kappa)$, where $\mathrm{K}(\kappa) = u(\pi/2,\kappa) = \int_0^{\pi/2} d\varphi/\sqrt{1-\kappa^2\sin^2\varphi}$. There are the useful following relations $\mathrm{sn}(u+\mathrm{K}) = \mathrm{cn}\,u/\mathrm{dn}\,u, \mathrm{cn}(u+\mathrm{K}) = -\sqrt{1-\kappa^2}\mathrm{sn}\,u/\mathrm{dn}\,u$, and $\mathrm{dn}(u+\mathrm{K}) = \sqrt{1-\kappa^2}/\mathrm{dn}\,u$.

In the particular case $\kappa \to 0$, the solutions simplify in sn $u \to \sin u$, cn $u \to \cos u$, and dn $u \to 1$. Another case of interest is when $\kappa \to 1$, for which sn $u \to \tanh u$ and cn $u = \mathrm{dn}\,u \to 1/\cosh u$.

B. (P, P') solutions (oscillating solutions)

Solutions of Eqs. (8) are chosen in the form

$$\begin{aligned}S_1 &= A\,\mathrm{sn}^2u + D,\\ S_2 &= B\,\mathrm{sn}\,u\,\mathrm{dn}\,u,\\ S_3 &= C\,\mathrm{cn}\,u,\end{aligned} \tag{36}$$

where $u = \Omega_J z$. This solution corresponds to the initial conditions in the Poincaré sphere $\vec{S}(0) = (D,0,C)^t = (D,0,\pm\sqrt{1-D^2})^t$. Substituting Eq. (36) into Eqs. (8) and using Eqs. (35), we obtain a set of algebraic equations

$$\begin{aligned}A\Omega_J = BC\Omega, \quad B\Omega_J = -2C(k+\Omega D),\\ B\Omega_J\kappa^2 = AC\Omega, \quad C\Omega_J = -2kB.\end{aligned} \tag{37}$$

In addition, the normalization of $\vec{S}$ gives

$$\|\vec{S}\|^2 = D^2 + C^2 = 1. \tag{38}$$

From Eqs. (37) and (38), we get the five parameters A, B, C, D, and Ω_J through κ:

$$D = -2\kappa^2\frac{k}{\Omega} \pm \sqrt{1-4\kappa^2(1-\kappa^2)\left(\frac{k}{\Omega}\right)^2}, \tag{39}$$

$$A = -2\kappa^2\left(\frac{k}{\Omega} + D\right), \tag{40}$$

$$B^2 = A^2/\kappa^2, \tag{41}$$

$$C^2 = -2\frac{k}{\Omega}A, \tag{42}$$

$$\Omega_J^2 = 4k\Omega\left(\frac{k}{\Omega} + D\right). \tag{43}$$

Equation (43) yields the condition $D + k/\Omega > 0$. The parameter D determines the initial point on the Poincaré sphere in the plane $S_2 = 0$, and then from Eq. (39), we can determine κ as a function of the initial point $D = S_1(0)$. The other parameters A, B, C, and Ω_J are then completely fixed with the initial condition $S_1(0)$. When κ changes from 0 to 1, the resulting $S_1(0)$ value changes from 1 to $1 - 2k/\Omega$ (the former value corresponds to the point P, while the latter one is exactly the magnitude of S_1 at the boundary between the two families of solutions in the plan $S_2 = 0$) in the case where $k < \Omega$. If $k > \Omega$, then when $S_1(0)$ changes from 1 to -1, the magnitude of κ varies from 0 to $\kappa_{\max}$ and after that decreases to 0 according to the dependence

$$\kappa^2 = \frac{1-D^2}{4(k/\Omega)(D + k/\Omega)}. \tag{44}$$

Let us now consider some limit and useful cases. First of all, we look for approximate solutions in the vicinity of the boundary between the two families of solutions. In this case, $(1-\kappa^2) \ll 1$ and $D \approx 1 - 2k/\Omega$. As previously, this solution exists if $k < \Omega$ because of the condition $D + k/\Omega > 0$. The other parameters can be easily found: $A \approx -2(1-k/\Omega), B \approx \mp 2(1-k/\Omega), C^2 \approx 4(k/\Omega)(1-k/\Omega)$, and $\Omega_J^2 \approx 4k(\Omega - k)$. Thus Eqs. (36) simplify to

$$\begin{aligned}S_1 &\approx D + A\,\tanh^2\Omega_J z,\\ S_2 &\approx B\frac{\sinh\Omega_J z}{\cosh^2\Omega_J z},\\ S_3 &\approx \frac{C}{\cosh\Omega_J z}.\end{aligned} \tag{45}$$

For the movement in the vicinity of P or P', we have $\kappa^2 \ll 1$. With $k < \Omega$, only the plus sign is suitable in Eq. (39). In this case, $D \approx 1 - 2\kappa^2(k/\Omega)(1+k/\Omega), A \approx -2\kappa^2(1+k/\Omega)$, $B \approx \pm 2\kappa(1+k/\Omega), C \approx \pm 2\kappa\sqrt{(k/\Omega)(1+k/\Omega)}$, and $\Omega_J \approx 2\sqrt{k(\Omega+k)}$. The previous set of parameters is also valid for $k > \Omega$ and corresponds to a movement around the point P. The solution with the negative sign in Eq. (39) is valid only for $k > \Omega$. The corresponding values for the parameters are $D \approx -1 + 2\kappa^2(k/\Omega)(k/\Omega - 1), A \approx -2\kappa^2(k/\Omega - 1)$, $B \approx \pm 2\kappa(k/\Omega - 1), C \approx \pm 2\kappa\sqrt{(k/\Omega)(k/\Omega - 1)}$, and $\Omega_J \approx 2\sqrt{k(k-\Omega)}$. This case corresponds to a movement around the point P' and is valid in the case $k > \Omega$. In both cases, we may use $\mathrm{sn}\,u \approx \sin\Omega_J z, \mathrm{cn}\,u \approx \cos\Omega_J z, \mathrm{dn}\,u \approx 1$, and the following approximate solutions can be used:

$$\begin{aligned}S_1 &\approx A\sin^2\Omega_J z + D,\\ S_2 &\approx B\sin\Omega_J z,\\ S_3 &\approx C\cos\Omega_J z.\end{aligned} \tag{46}$$

The last case of interest that we consider is with large natural anisotropy $k/\Omega \gg 1$. In this case, from Eq. (39), we get $\kappa^2 \ll 1$. The parameters become $D \approx \pm\sqrt{1-4\kappa^2(k/\Omega)^2}$, $A \approx -2\kappa^2(k/\Omega)$, $B \approx \pm 2\kappa(k/\Omega)$, $C \approx \pm 2\kappa(k/\Omega)$, and $\Omega_J \approx 2\sqrt{k(k-\Omega D)}$. We may use sn $u \approx \sin\Omega_J z$, cn $u \approx \cos\Omega_J z$, dn $u \approx 1$. The value of κ changes in the range $0 \leqslant \kappa \leqslant \Omega/(2k)$.

C. (Q, Q') solutions (rotating solutions)

Solutions of Eqs. (8) are chosen in the form

$$\begin{aligned}S_1 &= A\mathrm{sn}^2u + D,\\ S_2 &= B\mathrm{sn}\,u\,\mathrm{cn}\,u,\\ S_3 &= C\mathrm{dn}\,u,\end{aligned} \tag{47}$$

where $u = \Omega_J z$. This solution corresponds to the initial conditions in the Poincaré sphere $\vec{S}(0) = (D,0,C) = (D,0,\pm\sqrt{1-D^2})$. This solution exists only if $k/\Omega < 1$.

Following the same treatment as in the previous section, we obtain a set of algebraic equations

$$\begin{aligned} A\Omega_J = BC\Omega, \quad B\Omega_J = -2C(k+\Omega D), \\ B\Omega_J = AC\Omega, \quad C\Omega_J\kappa^2 = -2kB. \end{aligned} \tag{48}$$

The normalization of $\vec{S}$ also holds, leading to $D^2 + C^2 = 1$. The parameters A, B, C, D, and Ω_J can be written as a function of κ:

$$D = -2\frac{1}{\kappa^2}\frac{k}{\Omega} \pm \sqrt{1 + 4\frac{1}{\kappa^2}\left(\frac{1}{\kappa^2} - 1\right)\left(\frac{k}{\Omega}\right)^2}, \tag{49}$$

$$A = -2\left(\frac{k}{\Omega} + D\right), \tag{50}$$

$$B^2 = A^2, \tag{51}$$

$$C^2 = -2\frac{1}{\kappa^2}\frac{k}{\Omega}A, \tag{52}$$

$$\Omega_J^2 = \frac{4k\Omega}{\kappa^2}\left(\frac{k}{\Omega} + D\right). \tag{53}$$

Equation (53) yields the condition $D + k/\Omega > 0$. Finally, Eq. (49) can be written in the form

$$\kappa^2 = \frac{4(k/\Omega)(D + k/\Omega)}{1 - D^2}. \tag{54}$$

As in the last paragraph, D is related to the initial point in the Poincaré sphere, and then it is possible to link A, B, C, κ, and Ω_J to the initial value $S_1(0)$. When κ changes from 1 to 0, $S_1(0) = D$ varies monotonously from $(1 - 2k/\Omega)$ (the magnitude of S_1 at the boundary between the two families of solutions in the plan $S_2 = 0$) to $(-k/\Omega)$ (the magnitude of S_1 at the fixed points Q or Q'). To obtain the solutions for an initial point such that $-1 < S_1(0) < -k/\Omega$, it is necessary to change in the solution (47) the value u to $u + T/2$, where $T = 2\mathrm{K}(\kappa)$ is the spatial period (i.e., the beat length). Taking into account the properties of the Jacobi's functions given earlier, we obtain the solution

$$\begin{aligned} S_1 &= A\frac{\mathrm{cn}^2 u}{\mathrm{dn}^2 u} + D, \\ S_2 &= -B\sqrt{1-\kappa^2}\frac{\mathrm{sn}\ u\ \mathrm{cn}\ u}{\mathrm{dn}^2 u}, \\ S_3 &= C\sqrt{1-\kappa^2}\frac{1}{\mathrm{dn}\ u}. \end{aligned} \tag{55}$$

From the first Eq. (55), we obtain the relation between $S_1(0)$ and D for initial conditions in the plan $S_2 = 0$ in the case $-1 < S_1(0) < -k/\Omega$:

$$S_1(0) = A + D = -\left(2\frac{k}{\Omega} + D\right). \tag{56}$$

We can easily check that when D changes from $-k/\Omega$ to $1 - 2k/\Omega$, the parameter κ varies from 0 to 1 and the initial value $S_1(0)$ varies from $-k/\Omega$ (fixed point Q or Q') to -1 (fixed point P'). From Eq. (52), we get $C = \pm\sqrt{2|A|k/(\kappa^2\Omega)}$. The positive (negative) sign corresponds to a movement around Q (Q').

Let us now consider some special cases of interest. We start with the movement in the vicinity of the boundary between the two families of solutions. In this case, $(1 - \kappa^2) \ll 1$, and the parameters become $D \approx 1 - 2k/\Omega, A \approx -2(1 - k/\Omega), B \approx \pm 2(1 - k/\Omega), C \approx \pm 2\sqrt{(k/\Omega)(1 - k/\Omega)}$, and $\Omega_J^2 \approx 4k(\Omega - k)$. Finally, as one could expect, the approximate solutions take the same form as Eqs. (45).

For a movement in the vicinity of stationary points Q or Q', we have $\kappa^2 \ll 1 (k \neq 0)$, and the parameters simplify into $D \approx -k/\Omega + (\kappa^2/4)(\Omega/k - k/\Omega), A \approx -(\kappa^2/2)(\Omega/k - k/\Omega), B = \pm A, C \approx \pm\sqrt{1 - (k/\Omega)^2}$, and $\Omega_J \approx \sqrt{\Omega^2 - k^2}$. The approximate solutions are written

$$\begin{aligned} S_1 &\approx \frac{k}{\Omega} - \frac{A}{2}\cos 2\Omega_J z, \\ S_2 &\approx \pm\frac{A}{2}\sin 2\Omega_J z, \\ S_3 &\approx \pm\sqrt{1 - \left(\frac{k}{\Omega}\right)^2}. \end{aligned} \tag{57}$$

The last case of interest concerns an isotropic fiber. In this case, $k \to 0, \kappa \to 0$, and the parameters become $A = -2D, B = \pm A, C = \pm\sqrt{1 - D^2}$, and $\Omega_J = |C|\Omega$. The solution becomes a simple rotation around the poles Q and Q':

$$\begin{aligned} S_1 &= D\cos 2\Omega_J z, \\ S_2 &= \pm D\sin 2\Omega_J z, \\ S_3 &= \mp\sqrt{1 - D^2}. \end{aligned} \tag{58}$$

VI. NONLINEAR LOSSES

A. Derivation of the nonlinear transmission

The nonlinear evolution of the polarization along a fiber is commonly used to realize intensity-dependent losses in passively mode locked fiber lasers. It is therefore of great importance to determine optimal conditions leading to efficient modulation of the losses. In the ideal case are a vanishing transmission for low intensity (very high losses), a high transmission for high intensity (low losses), and a moderate switching power. The first property can be easily realized by considering a fiber length ℓ such that $k\ell = \pi$ placed between two crossed polarizers. The transmission is null in the absence of nonlinear effects. In fact, the first condition is realized each time $k\ell$ is an integer multiple of π. Our choice $k\ell = \pi$ is equivalent to considering a low-birefringent fiber, which is the case in the majority of experimental situations [11,29]. The realization of the second property will be achieved with a suitable orientation of the linear input polarization state. In the following, we consider therefore that the passing axis of the input polarizer is oriented along a direction doing an angle θ with the slow axis of the fiber. The output polarizer is therefore oriented along a direction with an angle $\alpha = \theta + \pi/2$. Although the Poincaré sphere is very convenient to study the evolution of the polarization state, it is not useful to describe the action of a polarizer because it is not merely a projection onto a vector in the equatorial plane. To simulate the action of a polarizer, we need

to use the Mueller matrices and the Stokes vectors. The Stokes vector $\vec{\mathcal{S}}$ is just a four-component vector built with the Stokes parameters defined in Eqs. (5). In such a formalism, the action of an optical component is modeled through a 4×4 matrix named the Mueller matrix. The Mueller matrix associated with a polarizer aligned with an angle α with Ox is written [30] as follows:

$$\underline{\mathcal{M}}(\alpha) = \frac{1}{2}\begin{pmatrix} 1 & \cos 2\alpha & \sin 2\alpha & 0 \\ \cos 2\alpha & \cos^2\alpha & \cos 2\alpha \sin 2\alpha & 0 \\ \sin 2\alpha & \cos 2\alpha \sin 2\alpha & \sin^2\alpha & 0 \\ 0 & 0 & 0 & 0 \end{pmatrix}. \tag{59}$$

The Stokes vector just after the input polarizer is

$$\vec{\mathcal{S}}(0) = \begin{pmatrix} 1 \\ \cos 2\theta \\ \sin 2\theta \\ 0 \end{pmatrix}. \tag{60}$$

The first component represents the intensity and is equal to unity, meaning that we are dealing with normalized quantities. The Stokes vector $\vec{\mathcal{S}}(\ell) = [1, S_1(\ell), S_2(\ell), S_3(\ell)]^t$ at the exit of the fiber is numerically calculated from Eqs. (8) because analytic solutions are not very useful for such calculations. Of course, the first component remains equal to unity because the fiber is considered lossless. Finally, the Stokes vector after the output polarizer is calculated by

$$\vec{\mathcal{S}}_t = \underline{\mathcal{M}}(\alpha) \cdot \vec{\mathcal{S}}(\ell). \tag{61}$$

The component of interest is only the first one, which represents the transmitted intensity. In addition, because we have taken a normalized input intensity, the first component directly gives the transmission of the system:

$$T = \tfrac{1}{2}[1 + S_1(\ell)\cos 2\alpha + S_2(\ell)\sin 2\alpha]. \tag{62}$$

The transmission T depends on the intensity (through the parameter Ω) and also on the orientation θ of the input polarizer. For the numerical simulations will be used $k = \pi$ and $\ell = 1$, except when other values are specified.

B. Optimization of the nonlinear transmission

We consider the evolution of the nonlinear transmission as a function of the input intensity or, more conveniently, as a function of the pumping parameter Ω. First of all, we can note that for $\theta = 0^\circ$ or $\theta = 90^\circ$, the transmission is null for any input power because the associated polarizations are eigenstates of the medium. The results are given in Fig. 12 for increasing values of the orientation angle of the input polarizer θ.

Results show that while θ increases from about 10° to 45°, the maximum transmission increases to reach unity for 45°. At the same time, the switching power, that is, the power needed to switch from 0 to the first maximum transmission, increases reasonably. We have checked that in the range 0°–45°, the trajectories in the Poincaré sphere remain far from the instability point P'. For $\theta > 45^\circ$, the nature of the evolution changes because the maxima are no longer equivalent since

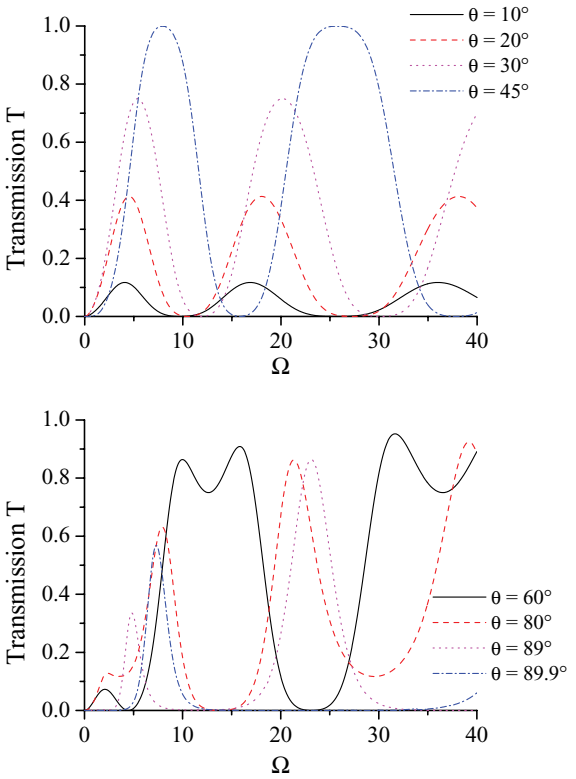

FIG. 12. (Color online) Evolution of the nonlinear transmission as a function of Ω for increasing values of the input polarization angle θ.

their amplitude strongly varies, the first being significantly lower than the second, thus rending the nonlinear switching less efficient than in the case $\theta < 45^\circ$, where all maxima are equivalent. In addition, when the input polarization approaches the unstable fast axis, the resulting nonlinear transmission becomes very sensitive to the exact value of θ, as pointed out in [24]. The repulsive behavior of P' is clearly evidenced in Fig. 13, which gives the evolution of the polarization state at the exit of the fiber in the Poincaré sphere for $\theta = 89^\circ$ and for increasing values of the pump parameter Ω. Indeed, as was pointed out in the stability analysis, the representative point is first attracted by P' then is ejected far from P'.

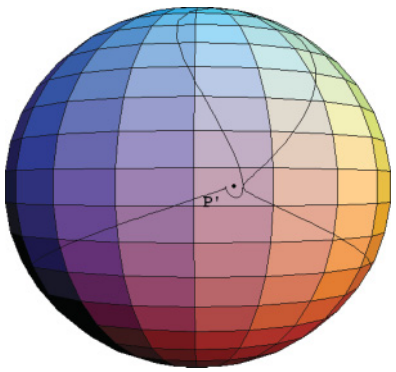

FIG. 13. (Color online) Evolution of the polarization state at the exit of the fiber in the Poincaré sphere as a function of Ω for an incident polarization close to the unstable fast axis, $\theta = 89^\circ$

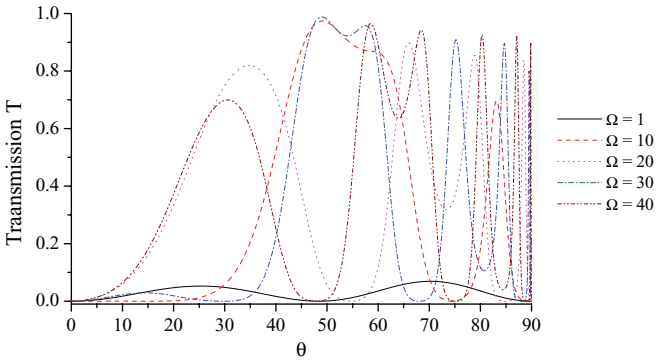

FIG. 14. (Color online) Evolution of the nonlinear transmission as a function of θ for increasing values of Ω.

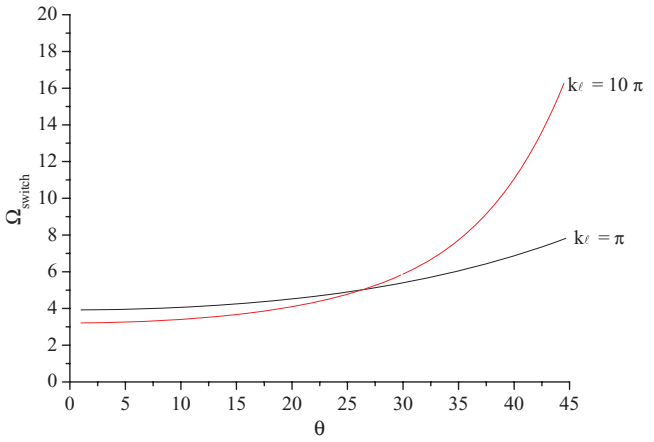

FIG. 15. (Color online) Evolution of the switching power parameter as a function of the incident polarization angle.

Additional physical insight is obtained with the evolution of the transmission as a function of the incident polarization angle θ. Results are given in Fig. 14 for different values of Ω. In the case $\Omega = 1(\Omega < k)$, the transmission undergoes low-amplitude variations, meaning that if the linear birefringence is greater than the nonlinear birefringence, the resulting nonlinear losses are not adapted for mode-locking applications. On the other hand, when $\Omega > k$, the nonlinear transmission is well contrasted, leading to potential efficient mode locking. In the range $\theta \in [30°,60°]$, the transmission exhibits a high maximum for a wide range of Ω, thus resulting in behavior compatible with mode-locking applications. Figure 14 also shows that the transmission suffers from a strong sensibility to the input polarization angle when approaching the unstable axis (except when $\Omega < k$, for which the fast axis is stable). Of course, such a situation is far to be desired for mode-locking applications.

The last parameter of great practical interest is the switching power defined previously. Because of the increasing sensibility of the nonlinear transmission for incident orientation beyond 45°, we restrict the range of variation of θ to $[0,\pi/4]$. Figure 15 gives the evolution of the switching pump parameter Ω_{switch} as a function of the incident polarization angle θ. For moderate linear birefringence $k\ell = \pi$, the switching power increases very slowly. It varies by a factor less than 2 when θ increases from 0° to 45°. On the other hand, for high birefringence fibers, the switching power increases considerably, leading to a great penalty when operating near $\theta = 45°$. This result is in agreement with the results reported in [23].

In summary, our results demonstrate that the optimal operating conditions for efficient nonlinear transmission, compatible with mode-locking applications, are a nonlinear birefringence greater than the natural birefringence and a linear input polarization oriented at about 45° from the slow axis of the fiber, although the switching power is slightly greater in comparison to the case $\theta = 0$. The modeling of the mode-locking properties in such conditions is left for further studies.

C. General case

In the last section, we considered a fiber placed between two crossed polarizers. A real experiment consists in a unidirectional ring cavity with a polarizer placed between two polarization controllers, as depicted in Fig. 16. The controller is generally composed of a set of half-wave and quarter-wave plates. After the polarizer, all the intensities have a well-defined linear polarization state parallel to the passing axis of the polarizer oriented with a direction making an angle α with Ox; the corresponding three-component Stokes vector is $\vec{S}^{+}$. At the entrance of the fiber, all the intensities have the same Stokes vector $\vec{S}(0)$ and are represented by a unique point in the Poincaré sphere. At the exit of the fiber, the optical Kerr effect leads to different polarization states for low and high intensities. We must therefore consider different representative points in the Poincaré sphere. The corresponding Stokes vectors are $\vec{S}_{\text{high}}(\ell)$ and $\vec{S}_{\text{low}}(\ell)$ for high and low intensity, respectively. Finally, just before the polarizer, the Stokes vectors are $\vec{S}^{-}_{\text{high}}$ and $\vec{S}^{-}_{\text{low}}$ for high and low intensity, respectively. Efficient mode locking requires high transmission for high intensities. The optimal value $T_{\text{high}} = 1$ is achieved if $\vec{S}^{-}_{\text{high}} = (\cos 2\alpha, \sin 2\alpha, 0)^{t}$, that is, if the polarization incident on the polarizer is parallel to its passing axis. Let us assume that the polarization controller 1 is adjusted in such a way that $T_{\text{high}} = 1$. The low transmission value associated with low intensity is

$$T_{\text{low}} = \tfrac{1}{2}[1 + S^{-}_{\text{low},1}\cos 2\alpha + S^{-}_{\text{low},2}\sin 2\alpha]. \tag{63}$$

This can be written in the condensed form

$$T_{\text{low}} = \tfrac{1}{2}[1 + \vec{S}^{-}_{\text{high}} \cdot \vec{S}^{-}_{\text{low}}]. \tag{64}$$

The phase plates are mathematically modeled through unitary transformations [31]. That means that a set of any phase plates conserves the angle between Stokes vectors for two incident polarizations. As a consequence, we have $\vec{S}^{-}_{\text{high}} \cdot \vec{S}^{-}_{\text{low}} = \vec{S}_{\text{high}}(\ell) \cdot \vec{S}_{\text{low}}(\ell)$. The low value of the transmission vanishes if $\vec{S}_{\text{high}}(\ell) \cdot \vec{S}_{\text{low}}(\ell) = -1$. Hence the maximum difference in the transmission is reached when the two representative points of the polarization states associated with low and high intensity are located on the opposite ends of any diameter of the Poincaré sphere. Under such circumstances, we have $T_{\text{high}} = 1$ and $T_{\text{low}} = 0$.

This property allows us to optimize the nonlinear losses. For example, let the natural birefringence be large, $k \gg \Omega$. If the

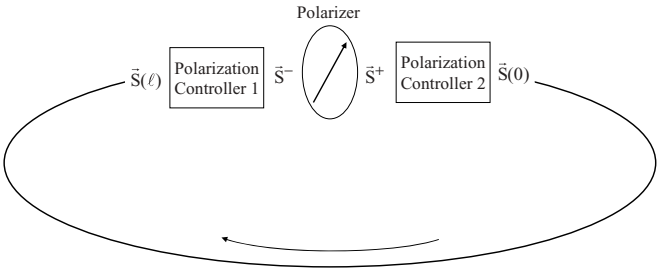

FIG. 16. Nonlinear birefringent fiber ring cavity with an intracavity polarizer placed between two polarization controllers.

polarization controller 2 is adjusted such that the initial point is in the vicinity of P or P', then during the propagation along the fiber, all points with different intensities remain near these points, as shown at the end of Sec. V B. As a consequence, $\vec{S}_{\text{high}}(\ell) \cdot \vec{S}_{\text{low}}(\ell) \approx 1$ and $T_{\text{high}} \approx T_{\text{low}}$; that is, the dependence of nonlinear losses on intensity is weak and is not suitable for passive mode locking. If the initial point on the Poincaré sphere is placed on the meridian plane $S_1 \approx 0$, then $D \approx 0$, and following Eq. (43), Ω_J does not depend on Ω. All points move at the same velocity because the nonlinear dependence is lost. As a consequence, the optimal condition is realized in the intermediate position $D \approx \pm 1/\sqrt{2}$ for which the difference in rotation velocity between low and high intensities is $\delta\Omega_J \approx \Omega/\sqrt{2}$. The efficiency of the nonlinear losses is of the same order of magnitude as in the case of a fiber without anisotropy $k = 0$, for which $\delta\Omega_J \approx |C|\Omega$, as has been demonstrated at the end of Sec. V C. It is obvious that the fiber should have the right length for which two points corresponding to high and low intensities could go away in Poincaré sphere at the greatest possible distance.

VII. CONCLUSION

In this article, we have revisited and fully analyzed the propagation of an electromagnetic wave in a birefringent fiber exhibiting optical Kerr nonlinearity. In the framework of Stokes parameters and the Poincaré sphere, we have determined the fixed points (i.e., the polarization eigenstates) and analyzed their stability. That allowed us to fully characterize the local topology of the solutions. Saddle-point instability has been confirmed in the case where the natural birefringence is lower than the nonlinear birefringence. Thanks to a conservation relation, we have established the formal mathematical analogy between the evolution of the polarization state and a particle moving in a potential well. Depending on both the initial conditions and the respective magnitude of linear and nonlinear birefringence, two potential wells are obtained. The first exhibits two minima, while the second has only one minimum. The potentials lead to the identification of two classes of solutions depending on the total energy of the equivalent particle. The first is a rotating solution for which the elliptical state of polarization rotates during propagation without changing the sign of the ellipticity. The second solution is an oscillating solution for which the sign of the ellipticity is periodically changed. In the Poincaré sphere, the two classes of solutions are separated by the separatrix, which is a double-looping curve crossing at the saddle point. The beat length has been determined in all cases of interest. Exact solutions have been found in terms of Jacobian functions. The two classes of solutions match at the separatrix.

The nonlinear losses associated with a nonlinear birefringent fiber placed between two crossed polarizers have been determined thanks to the Mueller matrices. We have identified the optimal conditions for efficient mode-locking applications. These conditions are a natural birefringence lower than the nonlinear one and a linear input polarization at about 45° of the slow axis of the fiber. We have then considered the general case of a ring fiber cavity with a polarizer placed between two polarization controllers. We have demonstrated that the maximum difference in the transmission for low and high intensities is achieved when the corresponding polarization states are located on the opposite ends of any diameter of the Poincaré sphere.

Our analysis is very important for understanding the laser dynamics in passively mode-locked fiber lasers based on nonlinear polarization rotation. It opens new interesting subjects of investigation such as the implication of the saddle instability on the operating regime of the laser. This is actually in progress. Another important study will be to perform the same analysis that we have done in this article for the more general case of an elliptical natural birefringence. Moreover, it will also be very interesting to perform an extensive investigation of the polarization dynamics associated with the modulational instability and soliton formation.

[1] H. A. Haus, K. Tamura, L. E. Nelson, and E. P. Ippen, IEEE J. Quantum Electron. **31**, 591 (1995).
[2] E. P. Ippen, Appl. Phys. B **58**, 159 (1994).
[3] M. Hofer, M. H. Ober, F. Haberl, and M. E. Fermann, IEEE J. Quantum Electron. **28**, 720 (1992).
[4] A. D. Kim, J. N. Kutz, and D. J. Muraki, IEEE J. Quantum Electron. **36**, 465 (2000).
[5] K. M. Spaulding, D. H. Yong, A. D. Kim, and J. N. Kutz, J. Opt. Soc. Am. **19**, 1045 (2002).
[6] B. Zhao, D. Y. Tang, L. M. Zhao, P. Shum, and H. Y. Tam, Phys. Rev. A **69**, 043808 (2004).
[7] N. N. Akhmediev, A. V. Buryak, J. M. Soto-Crespo, and D. R. Anderson, J. Opt. Soc. Am. B **12**, 434 (1995).
[8] P. Grelu, J. Béal, and J. M. Soto-Crespo, Opt. Express **11**, 2238 (2003).
[9] P. Grelu, F. Belhache, F. Guty, and J. M. Soto-Crespo, J. Opt. Soc. Am. B **20**, 863 (2003).
[10] E. Ding and J. N. Kutz, J. Opt. Soc. Am. **26**, 1400 (2009).
[11] H. Leblond, M. Salhi, A. Hideur, T. Chartier, M. Brunel, and F. Sanchez, Phys. Rev. A **65**, 063811 (2002).
[12] A. Komarov, H. Leblond, and F. Sanchez, Phys. Rev. A **71**, 053809 (2005).
[13] A. Komarov, H. Leblond, and F. Sanchez, Phys. Rev. E **72**, 025604(R) (2005).
[14] K. Tai, A. Hasegawa, and A. Tomita, Phys. Rev. Lett. **56**, 135 (1986).

[15] G. P. Agrawal, Phys. Rev. Lett. **59**, 880 (1987).
[16] L. F. Mollenauer, R. H. Stolen, and J. P. Gordon, Phys. Rev. Lett. **45**, 1095 (1980).
[17] S. Wabnitz, Phys. Rev. A **38**, 2018 (1988).
[18] G. Millot, E. Seve, and S. Wabnitz, Phys. Rev. Lett. **79**, 661 (1997).
[19] T. Chartier, A. Hideur, C. Özkul, F. Sanchez, and G. M. Stéphan, Appl. Opt. **40**, 5343 (2001).
[20] C. J. Chen, P. K. A. Wai, and C. R. Menyuk, Opt. Lett. **17**, 417 (1992).
[21] W. S. Man, H. Y. Tam, M. S. Demokan, P. K. A. Wai, and D. Y. Tang, J. Opt. Soc. Am. B **17**, 28 (2000).
[22] D. Y. Tang, L. M. Zhao, B. Zhao, and A. Q. Liu, Phys. Rev. A **72**, 043816 (2005).
[23] H. G. Winful, Appl. Phys. Lett. **47**, 213 (1985).
[24] H. G. Winful, Opt. Lett. **11**, 33 (1986).
[25] S. F. Feldman, D. A. Weinberger, and H. G. Winful, Opt. Lett. **15**, 311 (1990).
[26] D. Clarke and J. F. Grainger, *Polarized Light and Optical Measurement*, International Series of Monographs in Natural Philosophy, Vol. 35 (Pergamon Press, New York, 1971).
[27] B. Daino, G. Gregori, and S. Wabnitz, J. Appl. Phys. **58**, 4512 (1985).
[28] I. S. Gradshteyn and I. M. Ryzhik, *Table of Integrals, Series, and Products*, 5th ed. (Academic Press, New York, 1994).
[29] B. Ortaç, A. Hideur, T. Chartier, M. Brunel, C. Özkul, and F. Sanchez, Opt. Lett. **28**, 1305 (2003).
[30] P. Yeh and C. Gu, *Optics of Liquid Crystal Displays*, 2nd ed. (Wiley, New York, 2009).
[31] F. Sanchez, *Optique Non Linéaire* (Editions Ellipses, Paris, 1999).